4) With active caging of the spin vector along the case x-axis, it was possible to turn on the hemispheric torquor simultaneously with the spin torque. This usually resulted in much faster erection times than those indicated by Fig. 6.

Summary

The technique of active damping by hemispheric torquing results in much shorter ready times than other methods of damping free-rotor gyros. The experimentation that has been done with an air-bearing model indicates that the increased electronics complexity necessary to realize the method is small. The experiments with the model have successfully shown the ability of the gyro to completely invert the spin axis in the rotor automatically.

Although not presented here, fine damping using the optical flat has been shown to be mathematically feasible. The fine damping using a "D pattern" readout was not discussed, but has been done.

The expected reduction in damping time using active damping is at least of the order of 90%, and it is possible to design the system such that damping is completed simultaneously with spin-up.

References

[1] Lange, B., "The Unsupported Gyroscope," presented at the Unconventional Inertial Sensors Symposium, New York, Nov. 1964.

[2] Lange, B., "The Drag-Free Satellite," *AIAA Journal*, Vol. 2, No. 9, Sept. 1964, p. 1590.

[3] Lange, B. O., Fleming, A. W., and Parkinson, B. W., "Control Synthesis for Spinning Aerospace Vehicles Via the Property of 'Frequency Symmetry,'" *Journal of Spacecraft and Rockets*, Vol. 4, No. 2, pp. 142–150.

[4] Lange, B. O. and Fleming, A. W., "The Control of Linear Constant Dynamical Systems Which Are 'Frequency Symmetric' But Not 'Complex Symmetric,'" Paper 33A, Session 33, *Proceedings of the 1966 Congress of the International Federation of Automatic Control*, London, England, June 1966, pp. 33A. 1–33 A 12.

[5] Kryloff, N. and Bogoliuboff, N., *Introduction to Non-Linear Mechanics*, translated by S. Lefschetz, Princeton Univ. Press, Princeton, N.J., 1947.

[6] Fleming, A. W., "The Use of the Properties of Frequency Symmetry and Complex Symmetry in the Control of Linear Dynamical Systems," Ph.D. dissertation, Dept. of Aeronautics and Astronautics, Stanford Univ., Stanford, Calif.; also SUDAAR Rept. 266.

[7] Parkinson, B. W., "The Active Damping of Free Rotor Gyros," Ph.D. dissertation, May 1966, Dept. of Aeronautics and Astronautics, Stanford Univ., Stanford, Calif.; also SUDAAR Rept. 260.

JUNE 1970 J. SPACECRAFT VOL. 7, NO. 6

Experimental Studies of the Active Damping of Free-Rotor Gyroscopes

BRADFORD W. PARKINSON*
U. S. Air Force Academy, Colorado Springs, Colo.

AND

BENJAMIN O. LANGE†
Stanford University, Stanford, Calif.

This paper reports the experimental studies of a previously analyzed method of active damping of the nearly spherical rotor of a free-rotor gyro. The rotor must be damped (after spin-up) to spin about its axis of maximum inertia if rotor-fixed markings are used for readout. Both coarse ("hemispheric torquing") and fine active damping have been mechanized in an air-bearing gyro. The experimental damping characteristics agree well with the theoretical results and show that 1) damping to an accuracy of a few arc seconds can be completed in the same amount of time required to bring the rotor to operating speed, and 2) it can be accomplished so that the same side is always up, thus eliminating the necessity for the choice between two error models for the gyro or multiple start-up attempts until the correct side is up.

Nomenclature

E = coelevation angle between angular velocity vector of the rotor and the desired spin axis
h_μ, h_σ = lengths defined in Fig. 5
I_z = z axis moment of inertia
i_x = rms current in X or Y coil
i_{zx},i_{zy} = rms current in Z coil in quadrature with the X coil and the Y coil, respectively
K_m = experimentally determined coefficient giving torque/(amp)^2
K_p = polhode damper loop gain (cf. Ref. 2, p. 90)
K_δ = spin caging torque
k = l, V_{zy}/V, and V_{zx}/V for z, y, and x torques, respectively
L = coefficient of air drag resistance
$\mathbf{M}^+$,$\mathbf{M}^-$ = positive and negative torques, respectively
$\mathbf{M}_d$,$\mathbf{M}_e$ = disturbing and erection torques, respectively
$\mathbf{M}_h$ = undesired disturbing torque
$\mathbf{M}_{ht}$ = torquing signal from hemispheric torquer
$\mathbf{M}_{\max}$ = peak value of the torque
$\mathbf{M}_x$,$\mathbf{M}_y$,$\mathbf{M}_z$ = case x, y, and z axis torques, respectively
$\mathbf{M}_{xb}$,$\mathbf{M}_{xi}$ = average values of the torques along the x axis in the rotor and the x axis in the case, respectively

Received August 2, 1967; presented as Paper 67-590 at the AIAA Guidance, Control, and Flight Dynamics Conference, Huntsville, Ala., August 14–16, 1967; revision received September 29, 1969. The research reported here is part of a program supported at Stanford University by the U.S. Air Force under Contract AF33(615)-1411 from the Air Force Avionics Laboratory and is part of B. Parkinson's doctoral thesis.

* Member of Faculty, Department of Astronautics and Computer Science; Lt. Colonel, U.S. Air Force. Member AAIA.

† Associate Professor, Department of Aeronautics and Astronautics. Member AAIA.

N_0 = noise power per Hertz in the sensor output
n = number of teeth in rotor pattern
P_2 = normalized erection-torque expressed as erection acceleration/W_0^2
Q = $[(\phi_x - \beta_0) \bmod (2\pi/n)] - (\pi/n)$
R_1 = coil resistance, ohm
R'_2 = rotor resistance referred to stator, ohms
S_m = slip, percentage of Ω_s
T = period of one rotor revolution
T_j = rotor phase times; $T_1 = T/4$, $T_2 = T/2$, $T_3 = 3T/4$, and $T_4 = T$
t = time
t_i = time when hemispheric torquing is initiated
t_t = total time to complete coarse damping
V_x, V_y = voltages applied to x and y coils, respectively
W = rotor angular velocity
W_0 = effective zero-current rotor angular velocity due to gyro air torques
W_x, W_y, W_z = rotor-fixed components of rotor angular velocity
α_σ = arbitrary rotor initial phase angle
β_σ = angle from intersection of sensor locus and equator to the first down tooth (see Fig. 5)
Δ_{out} = average change in the output of the hemisphere sensor
δ = component of misalignment of spin-axis about the axis of the y sensor; see Fig. 9
ϵ_1, ϵ_2 = moment of inertia difference ratios for an unsymmetric rotor, $(C - A)/A$ and $(C - B)/B$, respectively, where A, B, and C' are the principal moments of inertia
η = defined in Fig. 9
θ_σ = $\sin(W_t - \alpha_\sigma)$; see Fig. 5
ϕ_σ = angle along rotor equator; see Fig. 5
χ = reactance of the coil (including the effect of the rotor)
Ω_s = excitation frequency of gyro coil current

Introduction

IN the companion paper[1] a scheme for the coarse phase of the active damping of the nearly spherical rotor of a free-rotor gyro is described and analyzed. Active damping is defined as making the torque axis of an erection field be a function of some component of rotor angular velocity in order to reorient the rotor's spin-axis direction to its axis of maximum moment of inertia while leaving its direction in a laboratory or inertial frame basically unaltered. This paper describes results of an experimental mechanization of active damping which comprises 1) coarse damping by "hemispheric torquing" [1] and 2) fine damping which achieves residual polhodes of only a few arcseconds.

In our hemispheric torquing scheme, the erection torque (applied perpendicular to the spin-up torque) averages to zero in inertial space; however, because the rotor is marked into hemispheres, and the erection torque switches direction with each half revolution of the rotor as a different hemisphere is sensed, the desired (coarse) rectification in the rotor's coordinates occurs. The fine-damping makes use of the fact that if a "dentate" pattern is applied along the equator between the hemispheres, the spin-axis readout contains a term whose amplitude is proportional to the polhode amplitude and which varies sinusoidally at polhode frequency. This term may be separated from the spin-axis-direction information by a low-pass filter which cuts off just above the polhode frequency and is used to command extra body-fixed moments which damp out the polhodes.

The experiments show that, beginning with a worst-case initial condition where the rotor is turned 180° away from the desired spin-axis, active damping can be completed in the same time that is required to bring the rotor up to speed, while achieving residual polhodes of ~5 arcsec amplitude.

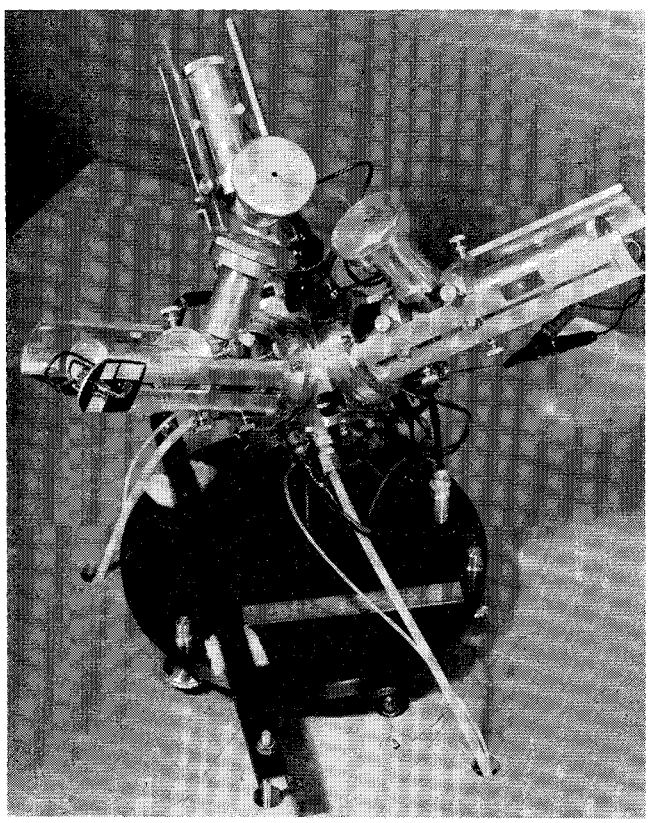

Fig. 1 Air-bearing model of the free-rotor gyro.

Description of the Apparatus

The gyro is shown in Fig. 1. Three orthogonal air-bearing pads are located in the lower three faces of the case tube. Each face contains a torquing coil (three orthogonal pairs in all). Orthogonal case axes designated X, Y, and Z are defined to lie parallel to the three long sensors attached to the gyro. In the laboratory reference frame, the z axis is the nominal spin axis and comes out of the figure to the left, the x axis comes out to the right, and the y axis goes into the figure and to the left. The spin-up coils, designated X and Y, have a 5-kc sine wave applied in quadrature and are used to generate a spin-up torque along the case Z axis. Each also creates one phase of the spinning field that generates torques along the X and Y axes. The other phase is supplied by currents in the Z coils. The X and Y torques are used for hemispheric torquing and spin-axis control. Current in the Z coil is switched and phased to provide these torques as called for by the control law.

The rotor (Fig. 2) is made of beryllium copper to minimize the possibility of permanent magnetism, which causes body-

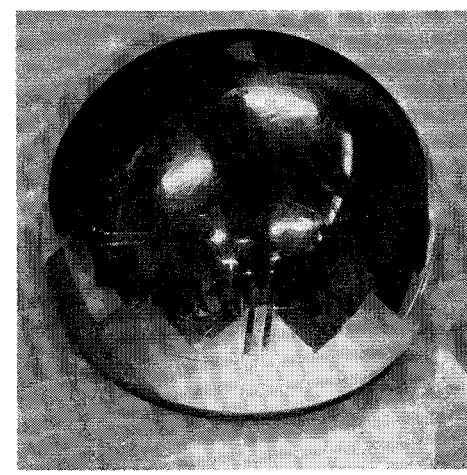

Fig. 2 Air-bearing gyro rotor made of solid beryllium-copper.

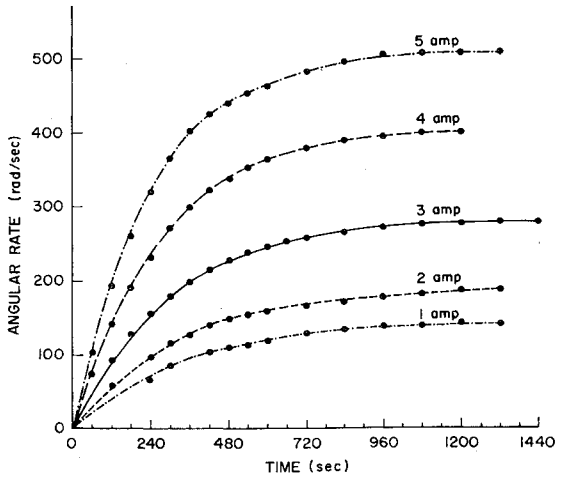

Fig. 3 Step-response curves for various rms current levels in the x and y coils of the air-bearing gyro motor.

fixed moments. Its diameter is 2.0000 ± 0.0001 in.; sphericity is better than 25μin. The measured moment-of-inertia difference ratio is 3×10^{-4}.‡

Notice the dull and bright "hemispheres"§ and the serrated markings of the "dentate" pattern. The axis of maximum inertia is perpendicular to the average equator.

The gyro is mounted on a $\frac{3}{4}$-in. aluminum plate secured to a concrete pier, and nitrogen is fed to the support pads from a regulated line which passed through holes in the aluminum plate. The gyro induction motor is excited with current at 5 kHz. Part of the z axis current is switched 180° in phase according to whether the z sensor detects a dull or a bright hemisphere. A frequency of 5 kHz was dictated by the number of teeth in the dentate pattern. Eleven teeth call for torque switching at 22 times per rotor revolution. At 3000 rpm this 5-kHz signal reverses roughly every three cycles. Any lower excitation frequency would place a very stringent requirement on the power amplifiers to effect phase reversal in the highly inductive coils. The maximum rotor spin speed is under 100 rps; therefore, the motor slip[3] is essentially constant for all operating speeds. The model of Section 221 of Ref. 3 is adequate for the experimental verification; in an air-bearing gyro, any uncertainty in the motor model is dwarfed by the uncertainty in air-bearing torques. The torque produced by the spin-up motor is due to the currents $i_x = i_y$ being in quadrature and is given by

$$M_m = \frac{V^2 R'_2}{2\Omega_s}\left[\frac{S_m(1+k)^2}{[R_1 S_m + R'_2]^2 + \chi^2 S_m^2} - \frac{(2-S_m)(1-k)^2}{[R_1(2-S_m) + R'_2]^2 + \chi^2(2-S_m)^2}\right] \quad (1)$$

For the spin rates considered, $S_m \cong 1$ and, since the coil reactances are nearly equal, $V_x/i_x = V_y/i_y = V_{zy}/i_{zy} = V_z i_x/_{zx}$. Therefore, the equations for torque become

$$M_z = K_m i_x^2,\ M_y = K_m i_x i_{zy},\ M_x = K_m i_y i_{zx} \quad (2)$$

The constant K_m has been separated from other air-bearing effects by assuming a model

$$M_z = K_m(i_x)^2 - L(W_r - W_0) \quad (3)$$

‡ It seems strange that a rotor so precisely machined would have a difference ratio this large. An unconfirmed conjecture is that the rotor was initially stamped, creating anisotropic internal stresses and a lack of homogeneity. A homogeneous rotor of this quality would probably have difference ratios of less than 10^{-5}.

§ The word "hemisphere" will be used in a general sense, because the dividing line may not be a simple "equator."

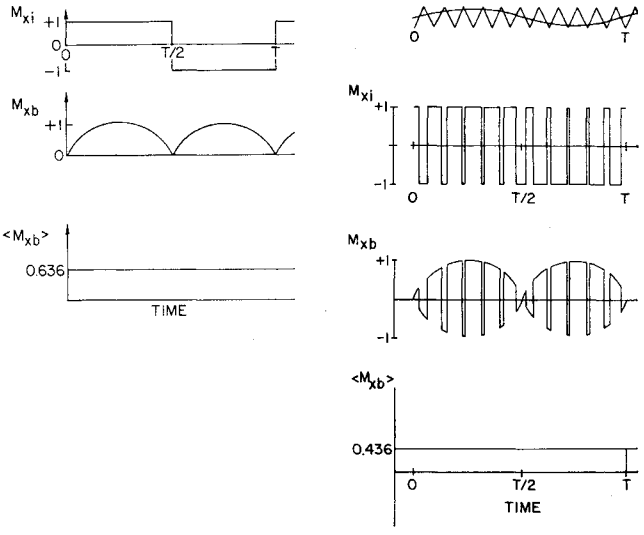

Fig. 4 Inertial and body-fixed torques for: a) large coelevation angles using single-axis hemispheric torquing, and b) small coelevation angles. Part b shows the reduction in average rotor-fixed torque as the sensor locus no longer clears points of the teeth; the top part of b shows the locus of the sensor through the dentate pattern.

The experimentally determined air-bearing motor step-response curves are shown in Fig. 3. The coefficients K_m and $1/L$ for the experiment were determined to be 0.059 ± 0.005 (rad/sec²)/(rms amp)², and (255 ± 10) sec, respectively.

Dentate Pattern and Active Caging

The rotor marking scheme must incorporate the dentate pattern and phase marking; it also should allow for some means of actively controlling the inertial spin-axis during hemispheric torquing, and it should be permanent, yet have negligible effect on the inertial properties of the rotor. In the dentate pattern in Fig. 2, the equally spaced teeth are formed from great circles crossing the equator at 45°. As coarse damping proceeds, a point will be reached at which the locus of the hemisphere sensor in the rotor no longer clears the points of the teeth. This condition leads quite naturally to the saturation type of control law which was postulated in the mathematical description for the digital simulation in Ref. 1. The point is illustrated by Fig. 4. Per the rule of hemispheric torquing, the X inertial torque is positive if the sensor is opposite the "northern" surface, or negative if it is opposite the southern one. For large E, the average body X axis torque is 0.636. As E decreases, the hemisphere sensor grazes the tops of the teeth, and there is a corresponding decrease in average torque amplitude. (Obviously, when the sensor is traversing the equator, there is no average effect.) This average is exactly the equivalent of the term $K_2 \sin(\theta^*)$ in the Kryloff-Bogoliuboff (KB) equations used in Ref. 1. When it goes to zero, it corresponds to

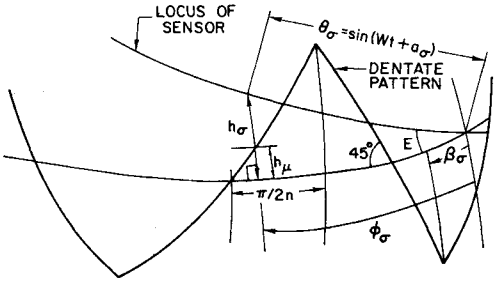

Fig. 5 Determination of height of point on sensor locus and tooth height of dentate pattern.

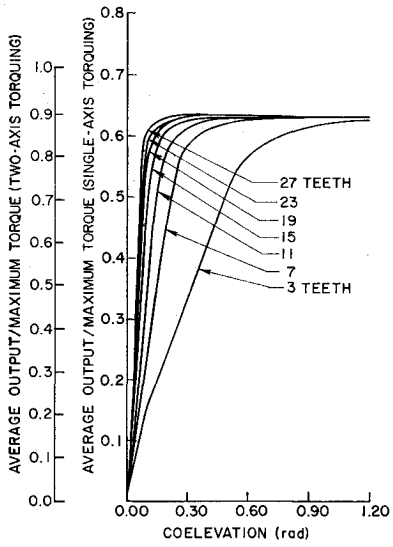

Fig. 6 Hemispheric-torquing saturation characteristic due to the dentate pattern.

zero input into the KB equations. Relative to E, the saturation-function characteristics will vary according to the number of teeth equally spaced around the rotor. If the great-circle locus of the hemisphere is determined using spherical trigonometry (see Fig. 5), the radian distance h_σ of the locus from the equator is

$$h_\sigma = \sin^{-1}[\sin E \sin(Wt + \alpha_\sigma)] \tag{4}$$

where W is the angular rate of the rotor and α_σ is an arbitrary initial phase. Similarly,

$$\varphi_\sigma = \tan^{-1}[\tan(Wt + \alpha_\sigma)\cos E] \tag{6}$$

where φ_σ is the distance along the rotor equator (rad). The height of the marker above the equator may be shown to be

$$h_\mu = \tan^{-1}[\sin(\pi/2n - |Q|)] \tag{7}$$

where $Q \triangleq [(\varphi_\sigma - \beta_\sigma) \bmod(2\pi/n)] - (\pi/n)$.

The average torque component along the rotor X axis is given by

$$\frac{\langle M_{xb}\rangle(\beta_\sigma,E,n)}{M_{\max}W/2\pi} = \int_0^{2\pi/W} \sin(Wt + \alpha_\sigma)\,\mathrm{sgn}[h_\sigma(E,t) - h_\mu(\beta_\sigma,t)]dt \tag{8}$$

The quantity $\langle M_{xb}\rangle$ has been evaluated for $\beta_\sigma = (2\pi/n)(j/8)$, where $j = 1, 2, \ldots, 7$, and averaged over this set of the β_σ for a fixed value of E. Taking $M_{\max} = 1$, the results are plotted in Fig. 6 as average torque $\langle M_{xb}\rangle$ vs coelevation E for various numbers of teeth n. The linear range of the saturation function vs n^{-1} is plotted in Fig. 7.

The value of having the saturation function rather than the pure on-off control is that it insures a stable null without limit cycles when the erection torque is properly adjusted and active spin-caging control is used. Active spin-caging

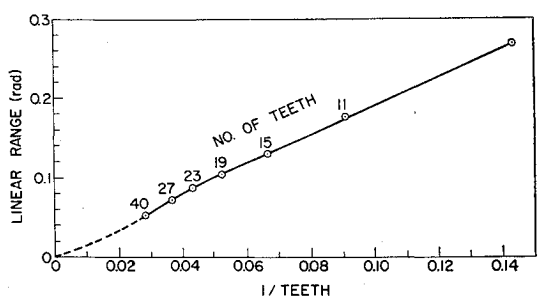

Fig. 7 Linear range of hemispheric torquer vs inverse teeth. The tooth edges are great circles crossing the equator at 45°.

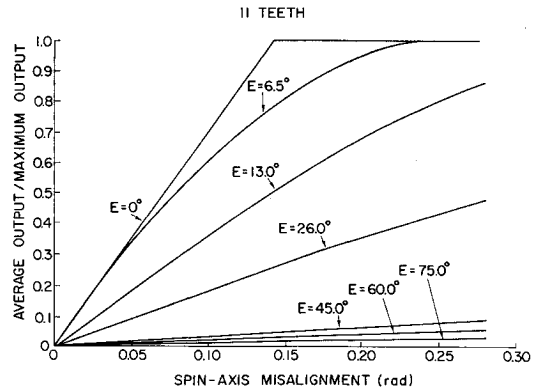

Fig. 8 Spin-axis misalignment sensitivities for various coelevation angles (E) using an 11-tooth dentate pattern.

control is achieved as follows. First we will only consider odd numbers of teeth, so that any great-circle locus of the sensor will have equal times in the "north" and "south," and the inertial X axis torque will average to zero. However, if the spin axis shifts slightly to or away from being perpendicular to the plane of the hemisphere sensor, while remaining fixed in the rotor, it causes the inertial average to become nonzero. The expression for this condition is

$$\frac{\langle M_{xi}\rangle(\beta_\sigma,E,n,\delta)}{M_{\max}W/2\pi} = \int_0^{2/\pi W} \mathrm{sgn}[h_\sigma(E,t,\delta) - h_\mu(\beta_\sigma,t)]dt \tag{9}$$

where the first-order approximation to $h_\sigma(E,t,\delta)$ is

$$h_\sigma = \sin^{-1}[\sin E \sin(Wt + \alpha_\sigma)] + \delta \tag{10}$$

where δ (rad) is the component of misalignment of spin-axis about the axis¶ of the y sensor, and α_σ may be taken as zero with no loss of generality in the averaging. Figure 8 shows $\langle M_{xi}\rangle$ vs δ (after averaging over the same set of β_σ as before) for various E's, with $n = 11$. For $E \geqslant 30°$, the teeth exert little influence on the average output, and they may be replaced with a single great circle (see Fig. 9) to estimate the effect of changes in spin-axis position on the average output. The average change in output (to first-order in δ) may be shown to be

$$\langle\Delta_{\text{out}}\rangle = \frac{2\eta}{2\pi}M_{\max} = \frac{\delta\cot E}{\pi}M_{\max} \tag{11}$$

where η is the angle defined in Fig. 9.

The method of spin-caging control, when damping is the large, is to use the average hemispheric torque as a measure of spin-axis misalignment to alter the direction of the spin-up field and thus reduce this uncertainty. If only the X axis control and Z axis spin-up torques are considered, the character of this control will be as revealed in Fig. 10. The Y axis

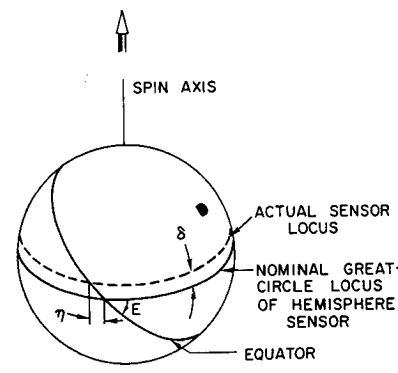

Fig. 9 The effect of spin-axis misalignment for large coelevation angles.

¶ The component about the x-sensor axis does not change the average output of the x sensor.

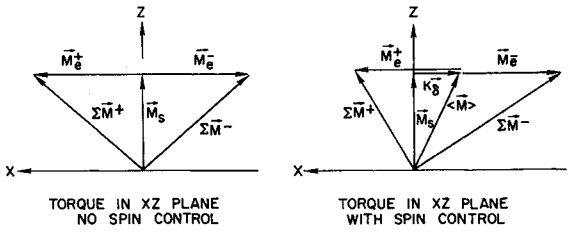

Fig. 10 Total torque in XZ plane with and without spin-caging control.

is controlled in an analogous manner. Thus, the addition of spin-caging control shifts the average torque direction but leaves the hemispheric torquing mechanism unchanged.

Unfortunately, Eq. (11) shows that the effect of misalignment changes sign for angles greater than $\pi/2$, so a spin-caging control with constant gain would have a destabilizing effect in this region. Use of the spin-axis sensor, located on the Z case axis, solves this problem. The sign of the spin-caging control gain is changed according to whether this sensor, on the average, sees the northern or southern hemisphere. This poses one additional problem, since the D-pattern will lead to improper decisions when the spin-axis is in it and under the spin-axis sensor. The solution to this problem is to use the fact that this condition implies that X and Y sensors are sensing a continuous dentate pattern. The condition that the dentate pattern is continuously present is used logically to override the decision based on Z-sensor output. Continuous dentate pattern is implied by the existence of the rotor phase times T_j. The control is diagrammed for the X channel in Fig. 11. A saturation function is included in the caging loop to allow the caging torque to exceed the hemispheric torque but not saturate the amplifiers.

An 11-tooth dentate pattern was selected for the model. It represents a compromise between torque-switching characteristics and saturation-function linear range. The pattern was modified as shown in the "polar map" of Fig. 12a; this allowed the event times to be determined logically independent of rotor spin speed. The logic scheme essentially counted state changes of one sensor during a continuous state on the other. If the number of state changes exceeded two, a phase time had occurred. Taken into consideration in this design modification were 1) the goal of symmetry of the pattern to insure that the spin-caging control is unbiased, and 2) the reduction of hemispheric-torquing biases by insuring that the modification does not bias any quadrant of the equator which would lead to body-rectified torques

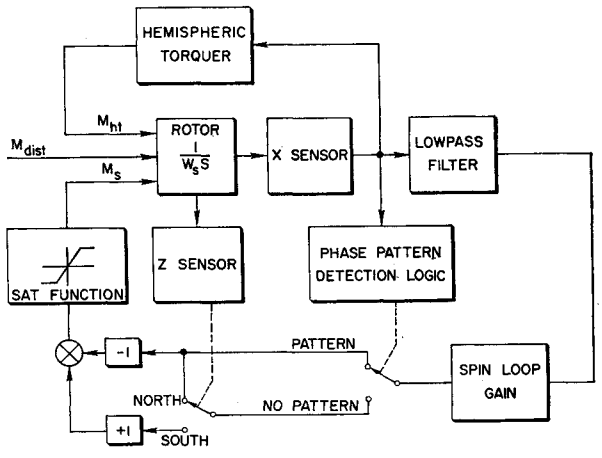

Fig. 11 Block diagram of X-axis spin-caging control. In the experiment the spin loop gain is set fairly high to reduce the effect of air-bearing turbine torques. The logical decisions illustrated are for active damping whose goal is the northern hemisphere along the positive Z case axis.

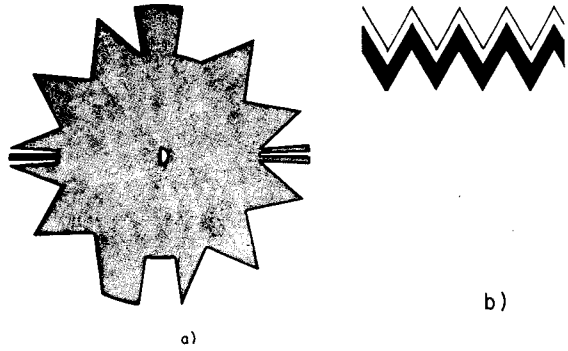

Fig. 12 Dentate pattern characteristics. Pattern (b) shows only a portion of the equator and is an alternative to marking (e.g., sandblasting) an entire hemisphere; the hemisphere is determined logically from the order in which the broad and narrow lines are sensed.

and a balance of the hemispheric torquer in an unintentional co-elevation offset.

For the air-bearing model, the rotor marking was determined using a procedure outlined in Appendix B of Ref. 2. The marking was applied by lightly sandblasting one hemisphere and placing the dentate-pattern on the other hemisphere. The best technique for actually marking the rotor is not obvious; this is an area which needs further exploration. An alternative scheme to completely marking the hemisphere is to duplicate the equatorial pattern with parallel wide and narrow lines (Fig. 12b). Digital logic could then be used to determine whether transitions were into the northern or southern hemisphere. The penalty for such a scheme would be in the area of increased electronics.

Optical Sensors and Electronics

The optical sensors for the experiment (Fig. 13) were designed for ease of operation and were much larger than needed for an actual gyro. The sensors for all three axes were the same except that the illumination and sensor field stops were larger for the Z axis sensor. The light source is a 6-v bulb, painted black, with a sandblasted circle on the bulb axis to pass the light. The sandblasting frosts the glass and reduces the possibility of filament vibrations affecting the system. Koehler illumination [Ref. 4, p. 508] is employed to insure uniform sensor response. This technique involves focusing the frosted glass on the objective lens with the illumination lens. In turn, the illumination stop is focused on the rotor using the objective lens. For the reflected light the focus point is the sensor stop after being reflected by the beam splitter. The sensor optics are the dual of the illumination optics in that the image of the photodetector (Fairchild FPM 100 phototransistor) is focused on the objective lens using

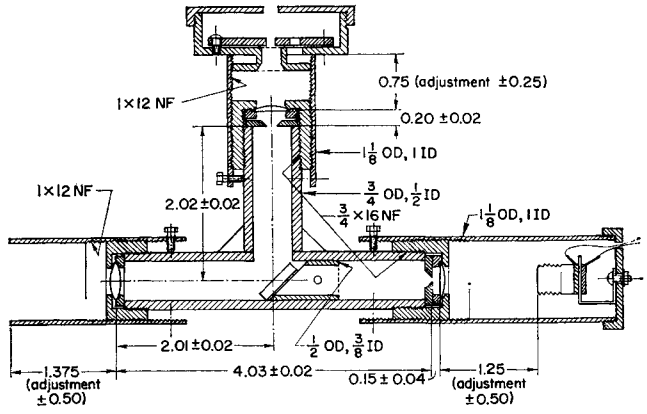

Fig. 13 Details of the optical sensor. The rotor would be to the left, the light source in the socket to the right.

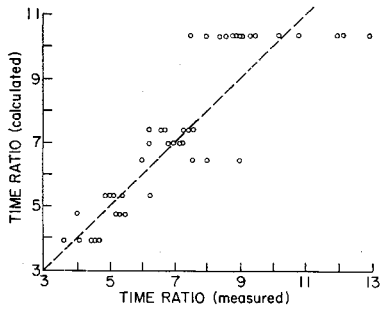

Fig. 14 Experimental damping times (sec) when damping simultaneously with initial spin up. Initially, the rotor is upside down in the case; the spin-up motor delivers a torque of 0.059 i_x^2 rad/sec.²

the sensor field stop lens. The photodetector and preamplifier are attached to the optical sensor in an enclosed housing. A second photodetector could be included to reduce thermal sensitivities, if necessary. It would form part of a bridge circuit by receiving a calibrated amount of light directly from the light source through fiber optics.

One minor design deficiency was the insufficient length of the beam splitter; minor secondary reflections were received in the photodetector, but, fortunately, did not prevent satisfactory sensor operation.

The system electronics[2] were designed and fabricated by the Stanford Inertial Instruments Laboratory. A detailed explanation of them is beyond the scope of this paper. Numerous switches and potentiometers were used to insure flexibility in the experiment, but they would not be needed for an operational free-rotor gyro. Using today's packaging techniques and components, the additional electronics needed to mechanize hemispheric torquing would be no larger than a cube 1.5 in. on a side.

Experimental Results

Hemispheric Torquing (Coarse Damping)

Three basic experiments were performed with the air-bearing model. The first was a measurement of actual damping times when the erection was delayed until $P_2 \leqslant 0.1$. This experiment provides a check of the analysis presented in Ref. 1. It is not normally the way that active damping should be applied, because it results in excessive damping time. The delay simulates the restriction on torquing due to the purely passive spin-axis caging which was used in this version of coarse damping. The formulas for rotor torque are used to find the time to complete damping in the large. Taking the minimum time after starting to spin-up for the initiation of hemispheric torquing,

$$t_i = \begin{cases} (10 i_{zz}/i_x{}^3 K_m)^{1/2} \text{ single-axis torquing} \\ (10.2^{1/2} i_{zz}/i_x{}^3 K_m)^{1/2} \text{ two-axis torquing} \end{cases} \tag{12}$$

The expected total time for the hemispheric sensors to reach

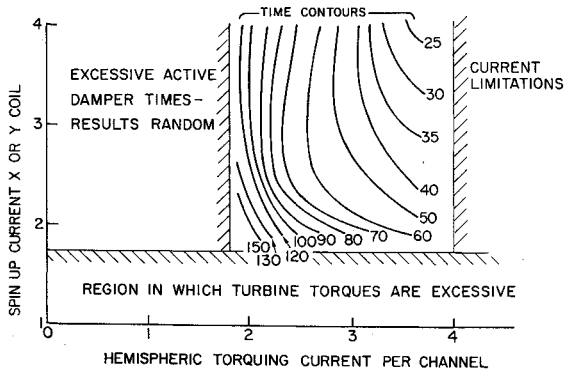

Fig. 15 Experimental results with simulated, passive caging.

the dentate pattern is derived from Ref. 1

$$t_t = \begin{cases} t_i \exp\left[\dfrac{(\pi - \text{sat})}{0.632} \dfrac{i_x}{i_{zz}}\right] \text{ single-axis torquing} \\ t_i \exp\left[\dfrac{(\pi - \text{sat})}{0.9} \dfrac{i_x}{i_{zz}(2)^{1/2}}\right] \text{ two-axis torquing} \end{cases} \tag{13}$$

where "sat" is the linear range of the saturation function due to the dentate pattern. The rotor was spun up to t_i without hemispheric torquing. As nearly as possible, this was done 180° away from the desired location in the rotor and approximately caged in the case. Hemispheric torquing was switched on at t_i and the time to reverse the rotor and start to obtain phase markings was recorded. Naturally the rotor took somewhat longer to stabilize completely, but the results could not be validly compared with the results of Ref. 1 due to the effect of the dentate pattern. Figure 14 compares calculated and measured time ratios, t_t/t_i. Because t_i was in the vicinity of 5 to 10 sec, the scatter in results is mainly attributed to the errors in t_i, for which the estimated rms error was 0.3 sec. The tendency for the theoretical prediction to be pessimistic for large time ratios is attributed to air-bearing turbine torques slowing the spin-up. These torques only become sizable for larger time ratios. The larger torques reduce the gyroscopic stiffness of the rotor, thus making the hemispheric torquer more effective.

The second experiment was the measurement of the time to damp in the large when active caging control is used and the hemispheric torquer is turned on simultaneously with spin-up. This approach results in shorter coarse damping times than the approach described in Ref. 1 and is only possible with spin caging control during spin-up. Damping times were checked against a digital simulation of the model which included the effects of amplifier saturation, the saturation function in the caging control, the saturation effect of the dentate pattern, and the effect of turbine torques. Because the rotor was turning very slowly, it was assumed to

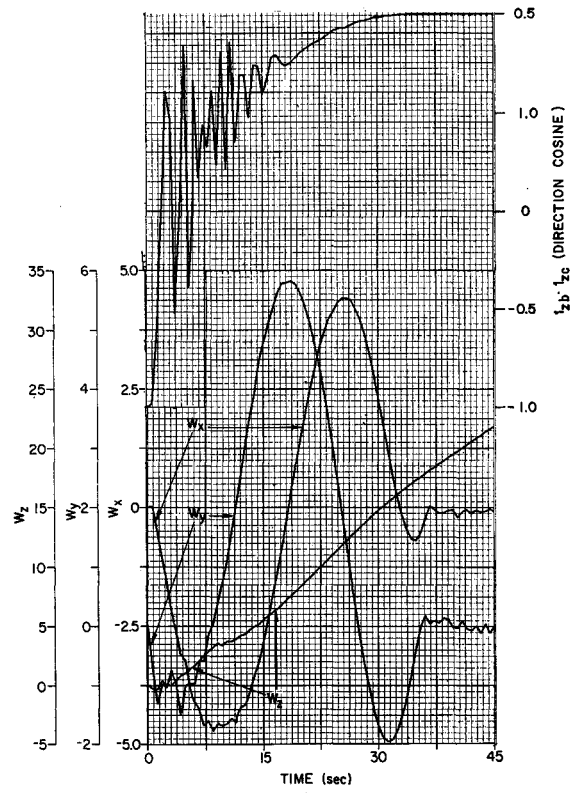

Fig. 16 Results of digital simulation of the air-bearing model. $E_0 = \pi$, $i_x = i_y = 3.0$ amp. The direction cosine starts at −1.0 (rotor upside down).

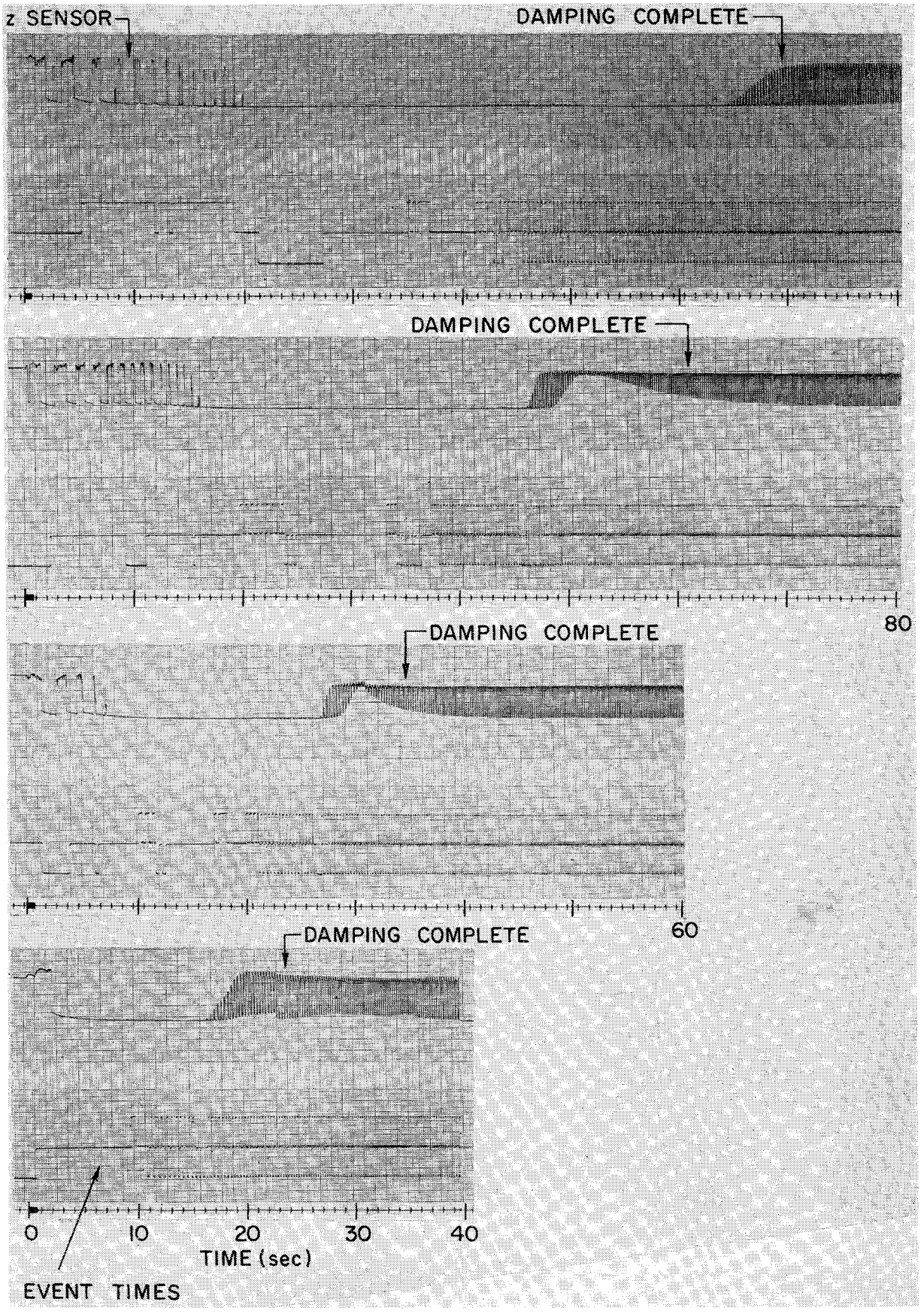

Fig. 17 Experimental run records for active caging. In each case the Z sensor first sees the wrong (bright) hemisphere, then the dull hemisphere, and finally senses the shiny D on the dull hemisphere. Damping in the large is complete when the steady D is being sensed and several seconds of the event times have been present, so the system may be shifted to fine damping.

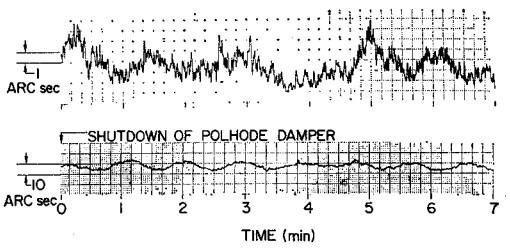

Fig. 18 Experimental traces during (top) and after (bottom) dentate-pattern polhode damping. The lower trace shows the capability of the polhode damper in spite of a 300 arc sec marking error on the rotor.

have a spherical moment-of-inertia ellipsoid in the simulation. The inputs to the simulation were the experimental values of current, motor characteristics, and other parameters of the experiment. Figure 15 is a plot of the experimental damping times using two-axis torquing for various values of torquing current. Figure 16 shows the results of the digital simulation for torquing currents $i_x = i_y = 3$ amp and $i_{zx} = i_{zy} = 3$ amp. Four of the experimental run records are shown in Fig. 17. Each is a run for different current levels. The Z sensor in each case starts opposite a point close to the pole of the shiny hemisphere. As damping proceeds, the sensor's locus moves into the dull hemisphere. The final high-frequency oscillations are due to the Z sensor receiving reflections from the shiny dentate-pattern. The event times from the logic output are also recorded. The four events are defined to be the times at which the rotor has rotated 90°, 180°, 270°, and 360°. One of the events is shown in the lower trace in each record. Each transition level represents an event. Figure 17 represents samples of a number of runs which were averaged for Fig. 15. Damping was judged complete when the fine damper had the signals necessary for its operation. The damping time for the digital simulation should be compared with the time to start sensing the dentate-pattern (Fig. 17b).

The experimental results are put in perspective if the total time to reach 1000 rad/sec for a spherical free-rotor gyro with similar rotor characteristics is calculated: $t = 1000/i_x^2(0.059)$. At $i_x = 4$ amp this is ~1000 sec, or ~30 times the active damping time. The reason for the shorter coarse damping times when the damper is turned on immediately is, of course, that it is easier to move the spin axis before it has built up speed.

The third experiment in the coarse mode performed with the air-bearing model was to allow the gyro to spin up, with the hemispheric torquer on, and stabilize so that there were only small residual motions of the angular velocity vector in the rotor. Then, using a Gaertner M101A microscope mounted on a Nikon cross-traveling micrometer stage, the small motions of the angular velocity vector in the rotor were measured, using the method developed in Ref. 5. The maximum oscillatory amplitude in the pointing direction of the angular velocity vector was 100 ± 20 arcsec. The hemispheric torquer was then turned off and the rotor, spinning at 2500 rpm, was allowed to polhode. The maximum polhode amplitude observed was 140 ± 20 arcsec. This result suggests that hemispheric torquing may have the potential of adequately damping the polhode motion with no need for fine damping.

Dentate Pattern Damping (Fine Mode)

With the rotor upside down, coarse damping and spin-up were initiated simultaneously; active caging was used. When the event times were occurring regularly (about 30 sec after start), the automatic delayed switch was started to change from coarse to fine damping (the delay was ~2 min). Spin-up was continued until a total of 12 min had elapsed, then the completion of the erection cycle was simulated by turning off the fine damper. The measure residual polhode amplitude indicated the quality of the initial alignment.

The primary expected sources of error were the "hangoff" (a torque switching at rotor frequency after the polhode is damped) of the polhode damper and the additive noise in the dentate pattern sensor. Because the free-rotor gyro is being modeled with the air bearing, the following additional undesired effects probably are present which would not be observed with an ESG or with an "unsupported gyro:"

1) Geometry-dependent turbine torques which have body-fixed components. These may be functions of air-bearing gas pressure, temperature, and the hemisphere to which the spin-axis is being erected.

2) As a result of earth rate and inertially fixed turbine torques, automatic spin-caging torques are quite large. Although the error signal is passed through a low-pass filter, it still may have body-fixed components.

3) A small amount of permanent magnetism has been measured on the Be-Cu rotor (0.6 mgauss). During operation, the magnetic dipole may move in the rotor leading to undesirable motion of the apparent maximum axis of inertia.

In spite of these effects, the fine damping consistently reduced the amplitude of polhode motion to 5 arcsec. Since the purpose of removing this polhoding is to eliminate perturbations on the spin-axis readout, it is natural to question the effect of 5 arcsec of polhode amplitude on a typical free-rotor gyro readout system. Since the polhode and spin frequencies typically differ by a factor of 10 or greater, the readout error should be an order of magnitude smaller ($\frac{1}{2}$ arcsec) or less. Furthermore, the polhode error magnitude due to hangoff is very nearly

$$e = M_h/I_z\beta^2(\epsilon_1\epsilon_2)^{1/2} \tag{14}$$

If it is assumed that the disturbance torque, including the additional effects mentioned previously, is primarily due to hangoff and that the experimental results are of a typical magnitude, then the effect on a hollow, free-rotor gyro may be estimated by considering that 1) the I_z of a hollow rotor is roughly one-tenth that of the model, 2) β is 3 to 10 times that of the model (model spins at 3000 rpm), and 3) ϵ is greater by about 100 (the model was 3.1×10^{-4}). The conclusion that the model's residual error may be expected to be reduced by a factor of 100 or more in an actual ESG probably will not be realized because of sensor output disturbance. If the main reason for the residual polhode is sensor noise, which will be assumed to be white and Gaussian, then the hangoff is

$$\text{rms error} = (3N_0K_p/2\beta\pi)^{1/2}$$

The point is that the effect of hangoff of the same magnitude will be less in most free-rotor gyros.

Typical experimental recordings are presented in Fig. 18. The upper trace shows the output of the Z sensor during the final stages of damping, and the lower trace (with a coarser

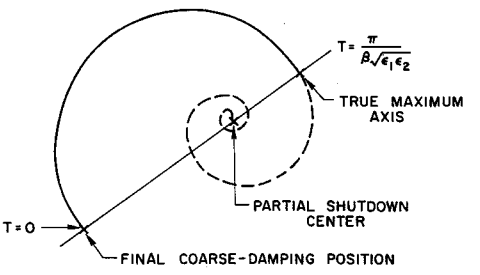

Fig. 19 The motion of the spin axis in the rotor during stutter shutdown. Coarse damping is partially shut down at $T = 0$; one-half polhode period later (when the spin axis is very close to the axis of maximum intertia) coarse damping is completely shut down.

scale) shows the residual polhode amplitude just after turning off the polhode damper. For the 26 experimental runs, the mean residual polhode amplitude was 5.6 arcsec, and the experimental standard deviation was 2.0 arcsec. Some sketchy experimental evidence indicates that it may be possible to eliminate fine damping. Hemispheric torquing and active caging will damp the polhode motion below levels that can be measured from the Z axis output. The rotor-fixed equilibrium position is not the maximum axis because of slight mismarking of the rotor and the consequent body-fixed torques. If the hemispheric torquer is turned off, after damping the polhode motion, the system will begin to polholde about a new equilibrium point, which is near the axis of maximum inertia but is not exactly aligned because of those effects discussed in the last section which are not due to the damping electronics. This motion, for all practical purposes, is undamped.

To eliminate fine damping, there are two possible approaches. One is simply to apply an additional torque, oscillating at rotor frequency, which has been carefully calibrated to cancel the body-fixed error torques caused by the hemispheric torquer. This method is relatively simple to implement and calibrate, but the apparent error may be slowly changing, so the validity of the calibration may be questionable. The second method is illustrated in Fig. 19. Rough experimental checks tend to establish the body-fixed perturbing torque (due to the polhode loop) as having a fixed direction with magnitude proportional to the hemispheric-torquing currents. If at some time $T = 0$, the hemispheric torquer is only partially shut down and then one-half polhode period later is completely shut down, the motion of the spin axis in the rotor would be as shown in Fig. 19. This technique will be called "stutter shutdown." If the model for the perturbing torque is correct, this method would work in spite of day-to-day changes in the effective torque error. At first thought, it would seem that the spin speed would affect the time of shutdown, but the number of rotor cycles per half period of polhode motion is $1/2(\epsilon_1\epsilon_2)^{1/2}$, an invariant quantity for low damping ratios. The disadvantage of stutter shutdown is that the initial calibration may be somewhat difficult. Initial experimental results indicate that polhode levels of less than 20 arcsec are possible. Both of these techniques should be considered in practical uses of the active damper because they help achieve a principal engineering goal of system simplicity.

Conclusions

The experiments have shown that active damping of a freely spinning spherical gyro rotor is practical, and a control law has been shown. The advantage in damping time compared to the times achieved by the methods of passive damping now used, is conservatively estimated to be an order of magnitude. Damping should always be completed by the time spin-up is complete. The slight differences between the theoretical results of Refs. 1 and 2 and the experimental results obtained with the air-bearing model can be attributed to two main effects: turbine torques developed by the air bearing, and uncertainties in the initial conditions. To use this method with a current ESG, no new sensors or coils are required. The increased volume of electronics would be small (<4 in.^{3}) with state-of-the-art techniques and could possibly be reduced by including a gyro spin-up mode in the guidance computer. For use in an ESG, the only major remaining question is how best to mark the rotor.

Hemispheric torquing can be used in either a single or a two-axis mode, but comparison with the time optimum for fixed erection-torque magnitude shows the latter to be the more effective by factors up to 2. For use with passive caging, the rotor should have some initial angular velocity to preclude instabilities. When this condition is met, an accurate formula for two-axis torquing is Eq. (13). Damping times of less than 25% of the time to spin up may be attained. A dentate rotor pattern was developed that allows a saturation type of damping control for the hemispheric torquer. (Its characteristic is superficially similar to a pattern developed at the University of Illinois for ESG readout,[6] but the use and readout of the dentate pattern are quite different.) Using the dentate pattern, and with very little added electronic complexity (and no additional coils or sensors, if dentate-pattern spin-axis readout is used), an active caging system (in the large) can be added, so that the hemispheric torquing may be initiated simultaneously with rotor spin-up.

After coarse damping alone, the polhode amplitude was only 140 arcsec. More precision in the marking scheme should allow this amplitude to be reduced by a factor of 2 or 3, which should be sufficient for many applications without recourse to a fine-damping system. A method of shutting down the hemispheric torquer, called stutter shutdown, offers promise of even smaller residual polhode amplitudes without recourse to fine damping.

It should be capable of reducing polhode motion to less than 5 arcsec. The theoretical results were confirmed by the experimental model. The average polhode amplitude after the damper was turned off was 5.6 arcsec.

Future Work

The active damper should be incorporated in an existing ESG, to be sure there is no incompatibility. The methods of marking the gyro rotor should be made to minimize the effect of markings on the inertia, mass unbalance, and dielectric properties. The possibility (indicated by a sketchy experimental check) of using a fixed time delay, rather than the Z-axis sensor, to switch the sign of caging gain should be investigated.

A detailed, quantitative investigation of the stutter shutdown technique should be performed to determine the exact shape of the spiral and to measure the equilibrium point vs hemispheric-torquing amplitude.

Application to Electrically Supported Gyroscopes (ESG's)

The rotor markings used herein were developed with two goals in mind: a) simplicity of construction for the laboratory electronics and b) possible application in an unsupported gyroscope[7] where (because the rotor is in free fall in space) the markings do not appreciably affect the drift rates. Application of this technique to conventional ESG's may require additional work. There are other methods (e.g., Fig. 12b) by which the hemispheres may be coded than by making the entire surface dull. An advantage of active damping is that one can always choose which hemisphere contains the "north" pole, whereas with magnetic or structural damping, the rotor may damp in with either side up. Thus, the active damper offers a considerably greater time saving than would be predicted merely by considering the ratio of damping time with a magnetic field to active damping time. In this connection, if the two hemispheres are canted on the rotor so that their dividing plane is at an angle of $\sim 45°$ with respect to the rotor's axis of maximum inertia, preliminary experimental results indicate that the hemispheric torquer will still tend to drive the spin-axis to that axis of maximum inertia in the rotor which is closest to the normal to the d viding plane if the hemispheric-torquer moments are not too large. Thus, in a strap-down ESG system which uses a great-circle cosine-readout system and which codes the hemispheres, hemispheric torquing could be used in conjunction with magnetic field damping to guarantee that the correct side always is up.

Finally, the fine damper was included in this study because it would be needed for an unsupported gyroscope.[7] For an operational ESG system, however, the primary advantage

of active damping is that the gyro always damps in with the same side up, and it probably would be best to omit fine damping and depend on either calibrating out the gyro marking error, using stutter shutdown, reducing the hemispheric-torquing moments at the end of the damping time so that the spin-axis is driven toward the maximum axis more than toward the effective pole of the markings, or using magnetic damping in connection with hemispheric torquing. Without fine damping, the complexity of the associated electronics for damping would be greatly reduced, because a sizable fraction of the electronics used in this experiment is already included in an ESG for initial spin-up and for spin-axis readout.

References

[1] Parkinson, B. and Lange, B., "The Active Damping of Free-Rotor Gyroscopes During Initial Spin-up," *Journal of Spacecraft and Rockets*, Vol. 7, No. 6, June 1970, pp. 667–675.

[2] Parkinson, B. and Lange, B., "The Active Damping of Free-Rotor Gyros," SUDAAR Report 260, May 1966, Dept. of Aeronautics and Astronautics Guidance and Control Lab., Stanford Univ.

[3] Skilling, H. H., *Electromechanics*, Wiley, New York, 1962, p. 369.

[4] Hardy, A. C. and Perrin, F. H., *The Principles of Optics*, McGraw-Hill, New York, 1932, p. 508.

[5] Planck, R. V., "Optical Flat Placement on Almost Spherical Gyro Rotors," Engineer's thesis, Aug. 1965, Dept. of Aeronautics and Astronautics, Stanford Univ.

[6] Baker, D. H. and Harrill, J. W., "Basic Principles of Unconventional Gyros," M.S. thesis, May 1954, Massachusetts Institute of Technology.

[7] Lange, B., "The Unsupported Gyroscope," *Proceedings of the 1964 Unconventional Inertial Sensors Symposium*, New York, Nov. 1964.

JUNE 1970 J. SPACECRAFT VOL. 7, NO. 6

Mariner Limit Cycles and Self-Disturbance Torques

B. DOBROTIN* AND E. A. LAUMANN†
Jet Propulsion Laboratory, Pasadena, Calif.

AND

D. PRELEWICZ‡
California Institute of Technology, Pasadena, Calif.

Details of the Mariner attitude control system limit cycle operation during cruise are presented. Limit cycle operation is shown to vary from the ideal case to single side operation. The data are analyzed to determine the form of the variation and to seek an explanation. The results show that there is a bias torque of several dyne-cm which changes at the end of a limit cycle, coinciding with the firing of an attitude control jet. Diagrams illustrate the various limit-cycle operations and the changes encountered. Because Mariner V had a balanced sun profile, the solar bias was low and it appeared that much of the disturbance torque was self-generated. An analysis of the attitude control jets demonstrated that a sizable torque could be generated by leakage through the attitude control valves. Experimental data obtained confirmed this suspicion.

Nomenclature

A = nozzle throat area
F = force (thrust)
G = gravitational acceleration
I_{sp} = specific impulse of jet
k = Boltzman constant
l = jet couple length
m = mass of molecule
$\dot{M}$ = mass flow rate
n = molecules number density
n_v = molecular number density having a velocity, v
$\dot{N}$ = molecular number rate
P = pressure
T = temperature
$v,\bar{v}$ = molecular velocity and average molecular velocity
$\dot{V}$ = gas volumetric flow rate
λ = mean free path length
ρ = gas density
θ = angle between nozzle centerline and molecular velocity vector
ψ = nozzle expansion half angle
σ = molecular collision cross section
τ = attitude control torque
ϕ = momentum of molecule

Subscripts

0 = all molecules
1 = molecules that do not impact nozzle
2 = molecule that impacts nozzle
s = gas supply conditions

Presented as Paper 69-844 at the AIAA Guidance, Control and Flight Mechanics Conference, Princeton, New Jersey, August 18–20, 1969; submitted August 18, 1969; revision received March 9, 1970. This work presents the results of one phase of research carried out at the Jet Propulsion Laboratory, California Institute of Technology, under Contract NAS 7-100, sponsored by NASA.

* Project Engineer, Spacecraft Control Section, Guidance and Control Division. Member AIAA.

† Member, Technical Staff, Environmental Sciences Division. Member AIAA.

‡ Doctoral candidate.

Introduction

THE Mariner series of spacecraft is designed for trips to Venus and Mars. Since 1962, five Mariners have been successfully launched; two were sent to Venus and three